IET Microwaves, Antennas & Propagation

Research Article

IET Journals
The Institution of Engineering and Technology

Three-dimensional profiling of collimated radio-frequency orbital angular momentum beams

ISSN 1751-8725
Received on 17th September 2019
Revised 17th September 2019
Accepted on 10th February 2020
doi: 10.1049/iet-map.2019.0808
www.ietdl.org

Joshua K. Hamilton[1,2] ✉, Simon J. Berry[2], Joseph H. Spencer[2], Christopher R. Lawrence[2], Francis C. Smith[2], Timothy D. Drysdale[3,4]

[1]*Department of Physics and Astronomy, University of Exeter, Exeter, Devon EX4 4QL, UK*
[2]*QinetiQ Ltd, Cody Technology Park, Farnborough GU14 0LX, UK*
[3]*The Open University, Walton Hall, Milton Keynes MK4 2BB, UK*
[4]*School of Engineering, Institute for Digital Communications, University of Edinburgh, Edinburgh, Scotland EH9 3FG, UK*
✉ *E-mail: J.Hamilton2@exeter.ac.uk*

Abstract: The use of orbital angular momentum (OAM) modes in radio communication is thought to enhance capacity. This work focuses on using the $l = +1$ mode transmitted from a 180 mm diameter, 8-element circular antenna array. The transmitted OAM beam was collimated by using a spherical mirror and the intensity and phase were investigated. A *xyz* scanning stage was used to profile the propagating OAM beam in three dimensions, resulting in a detailed investigation into the effects of collimation on the OAM beam. The proposed system was shown to reduce the beam divergence from 36.6° to 1.2°, without affecting the OAM mode purity of the beam for a frequency range of 4–6 GHz. This investigation showed a step towards realising practical control over the divergence of OAM-carrying beams.

1 Introduction

It is well known that electromagnetic fields can transport angular momentum as well as linear momentum via the use of beams with helical phase wave fronts [1]. However, the generation of photons in pure orbital angular momentum (OAM) states was not possible until certain advances in optical techniques were made [2–5]. In the last decade, there has been a vast amount of interest in translating the basic physical concept of OAM from optics to radio. In 2007, Thidé *et al.* [6] presented the first simulations of radio-based OAM, sparking the interest of the radio communications community. Since this initial work, many methods of generating OAM modes have been proposed. Such methods include: holographic plates [7, 8], spiral phase plates [8–10], resonator-based systems [11], inhomogeneous birefringent devices [12], and uniform circular arrays (UCAs) [13–15]. The interest has arisen because OAM could be used to improve the spectral efficiency of communication by multiplexing parallel data streams using OAM modes at the same frequency. Other possible applications exist in radio astronomy research – for example: exoplanet detection, radar probing of the Sun, and in the detection of ultrahigh energy neutrinos.

However, for OAM modes (other than the traditionally used plane wave $l = 0$ mode), a vortex occurs along the boresight of the antenna (the centre of the beam). For increasing OAM modes, the divergence angle of the beam increases. As a result, the transmission over long distances would not be guaranteed. Also, the receiver aperture size required for optimum reception scales with the OAM mode [16] and link distance, reaching impractical values for long-distance communications. Due to this crucial issue, many practical applications that require the OAM beam to be transmitted over long distances are being held back.

Notable work by Tamburini *et al.* [17] focused on using a split parabola antenna to generate a single OAM mode. The beam collimation due to the parabola resulted in a reduction of the beam divergence.

Interest has been shown in controlling the divergence of OAM beams generated by a UCA due to the appeal of multiple mode generation. The divergence of an OAM beam produced by a UCA can be controlled by increasing the diameter of the array [13]. This method is successful until the limit where the antenna array sizes become impractical. More recently, the range of an OAM radio link has been shown to be improved by combining a UCA with a graded index lens [18, 19]. The use of graded index lenses showed promise by reducing the divergence angle by 57%. However, each system requires a tailor-made lens that could be impractical for many real-world applications. Apart from within this handful of studies there is relatively little discussion of beam collimation in the open literature.

2 Methods

The OAM transmit array consisted of an 8-element array of 5 GHz (optimal range 4.920–5.925 GHz) ISM, WiFi antennas, mounted on a Perspex stand (see Fig. 1 inset). A benefit of these highly efficient (∼88%) antennas is that they are readily available commercially (2J0A02-5.0-C151G, *2J Antennas).* The circular OAM array had a diameter of 180 mm, mounted to a 350 mm diameter Perspex backing. The antenna array was designed in such a way that the transmitter could be controlled by a single feed – the output of a vector network analyser (VNA). To achieve this, an eight-to-one power divider was used to feed the phase shifters. Programmable phase shifters were used to impose the appropriate phase shifts to create the OAM modes, as well as to compensate for the slight differences in the path lengths of the antennas. The phase shifters and antennas were controlled using LabVIEW. This system was able to generate OAM modes $l \in \{0, \pm1, \pm2, \pm3\}$; however, in the work presented here the incremental phase shift between adjacent WiFi antennas was set to 45° in order to produce an OAM $l = +1$ mode for a range of frequencies (4–6 GHz). A schematic diagram of the experimental setup is shown in Fig. 1.

The setup comprised the UCA transmitting an OAM beam with $l = +1$ onto the collimating device, in this case a standard offset reflector. Whilst any radio frequency-reflective surface would suffice (e.g. reflective fabrics [20] or satellite dishes [21]) if appropriately shaped, we chose to use a pre-existing spheroidal mirror held within our laboratories, positioned 1.8 m away from the UCA. The mirror was made of an aluminium alloy with a diameter of 1.8 m. The dimensions of the mirror resulted in a focus length of ∼1.5 m. When the beam was reflected from the mirror the handedness of the beam was reversed, therefore resulting in an OAM $l = -1$ beam. The beam was then directed towards a *xyz* stage

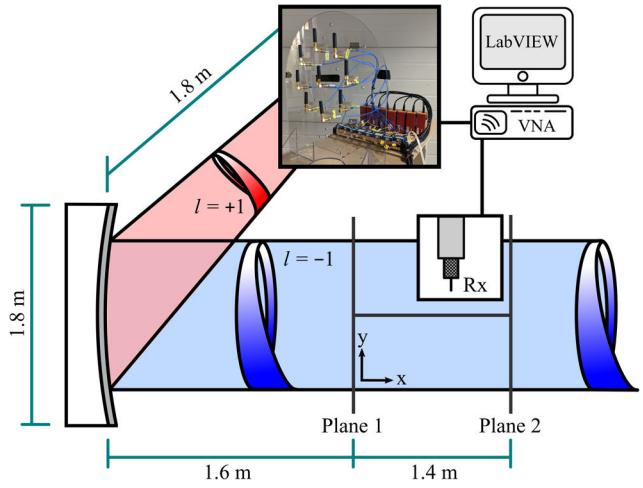

Fig. 1 *Schematic diagram of the experimental setup, showing a photograph of the 8-element circular array connected to a VNA and the computer running the LabVIEW software. The array is transmitting the l = +1 OAM mode beam onto a spherical microwave mirror. Plane 1 and Plane 2 depict the y–z plane scans and the line connecting them depicts the x–z plane scan. A diagram of the coaxial cable receiver (Rx) is also shown. Figure not drawn to scale*

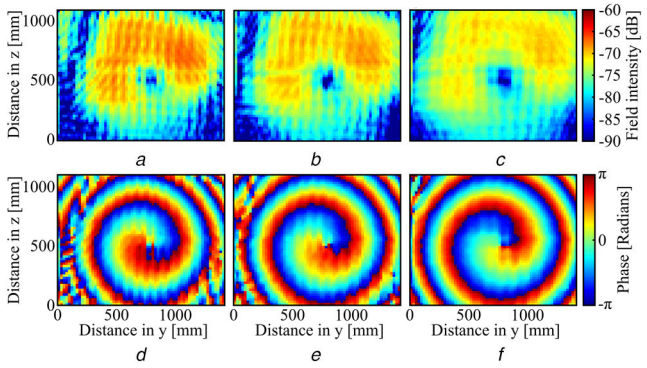

Fig. 2 *Measured results from the field scan of the 5 GHz, l = +1 OAM mode beam in the y–z plane, to visualise the divergence of the beam*
(a) Scans were conducted at zero position, ***(b)*** Additional distance of 0.25 m, ***(c)*** Additional distance of 0.50 m, ***(d)*** Phase patterns at zero positon, ***(e)*** Additional distance of 0.25 m, ***(f)*** Additional distance of 0.50 m

field scanner (placed 1.6 m away from the microwave mirror), which was able to probe the field intensity and phase profile of the beam in a given volume. The probed volume of interest was ∼1.4 m × 1.5 m × 1.0 m (i.e. $x \times y \times z$). As a result, the beam had travelled a total distance of 4.8 m at the furthest plane measured. The Fraunhofer (far field) distance for the antenna is 86 cm at 4 GHz and 130 cm at 6 GHz, placing the measurements in the far field. The field scanner comprised a simple stripped piece of semi-rigid coax connected to a high-precision microwave cable. The stripped portion of the coax and the additional shielding are orientated parallel and perpendicular to the incoming *E*-field, respectively. The field scanning technique used has been previously validated [22]. The probe was programmed to raster scan in a given plane. Three scans were taken in this investigation. The scans consisted of two *y*–*z* planes scans, separated by 1.4 m, as well as a scan along the *x*–*z* plane along the centre of the beam.

3 Results and discussion

To visualise the divergence of the OAM beam, a standard $l = +1$ OAM mode beam was generated using the UCA at 5 GHz. Three scans (in the *y*–*z* plane) are shown in Fig. 2; the separation between each scan was 0.25 m. For the non-collimated beam, there was an increase in the diameter of ∼28% over the total distance (0.50 m). Figs. 2*d*–*f* show the characteristic chiral phase pattern for a standard $l = +1$ OAM mode beam.

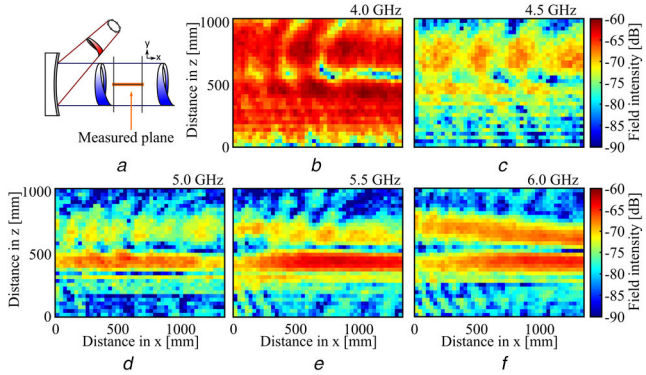

Fig. 3 *Measured field intensity from the 4–6 GHz field scan, l = −1 OAM mode beam in the x–z plane*
(a) Schematic diagram showing the measured plane, ***(b)*** Field intensities for 4 GHz, ***(c)*** Field intensities for 4.5 GHz, ***(d)*** Field intensities for 5 GHz, ***(e)*** Field intensities for 5.5 GHz, ***(f)*** Field intensities for 6 GHz
The zero in the *x*-axis is positioned 1.6 m away from the microwave mirror

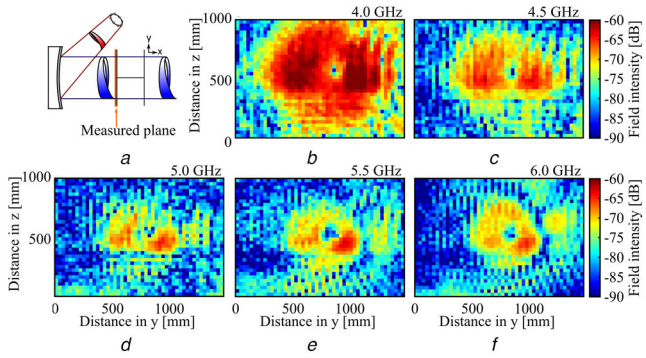

Fig. 4 *Measured field intensity from the 4–6 GHz field scan, l = −1 OAM mode beam in the y–z plane. The scan was taken at 1.6 m away from microwave mirror (Plane 1)*
(a) Schematic diagram showing the measured plane, ***(b)*** Field intensities for 4 GHz, ***(c)*** Field intensities for 4.5 GHz, ***(d)*** Field intensities for 5 GHz, ***(e)*** Field intensities for 5.5 GHz, ***(f)*** Field intensities for 6 GHz

The field intensity in the *x*–*z* plane, in the case when the OAM beam has been collimated is shown in Fig. 3 for a range of frequencies. The pseudo-colour plot shows the field intensity in a log scale with arbitrary units. When an antenna transmits an OAM beam into free space the beam strongly diverges with a null on boresight (as shown in Fig. 2), unless $l = 0$ is transmitted (a plane wave). For all frequencies, at ∼540 ± 30 mm in the *z*-direction the characteristic null along the beam's centre can be observed for the full distance measured. However, the observed divergence of the beam is minimal and the broadness of the null is tightly confined, compared to the standard divergent beam (without the mirror). As the frequency of the beam is increased the tightness of the beam is increased, ranging from an approximate diameter of 1000–480 mm at a distance of 4.8 m.

For further analysis of the spread of the beam shown in Fig. 3*d*, the initial dimension (after the beam has propagated 1.6 m from the mirror) in the *z* direction is shown to be ∼720 ± 15 mm. After propagating a further 1.4 m, the beam has a *z* direction diameter of 690 ± 15 mm (Fig. 4*d*). This demonstrates the tight control over the uniformity of the beam as it propagates through free space.

Fig. 4 shows the measured field intensity for the *y*–*z* plane at the position Plane 1 (1.6 m away from the microwave mirror) for the frequency range of 4–6 GHz. The figure clearly shows the field intensity profile of an OAM $l = -1$ beam, with a visible vortex in the centre resulting in a minimum in field intensity.

It is not only important for the vortex and beam divergence to be investigated but also the phase pattern of the beam. The phase pattern was investigated to ensure that the collimation method had not affected the characteristic structure of the OAM beam.

Fig. 5 shows the measured phase pattern at position Plane 1 and the pseudo-colour plot shows the phase in degrees. The phase

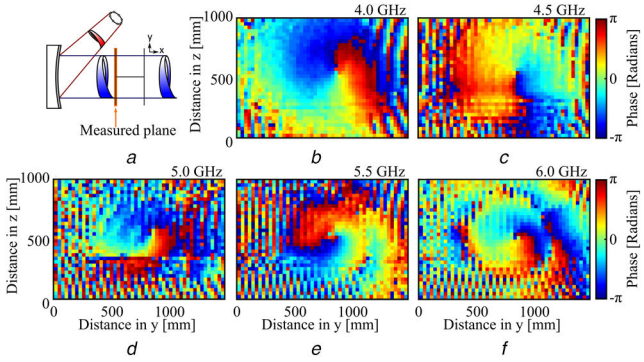

Fig. 5 *Measured phase pattern from the 4–6 GHz field scan, $l = -1$ OAM mode beam in the y–z plane*

(a) Schematic diagram showing the measured plane. The scan was taken at 1.6 m away from microwave mirror (Plane 1), ***(b)*** Field intensities for 4 GHz, ***(c)*** Field intensities for 4.5 GHz, ***(d)*** Field intensities for 5 GHz, ***(e)*** Field intensities for 5.5 GHz, ***(f)*** Field intensities for 6 GHz

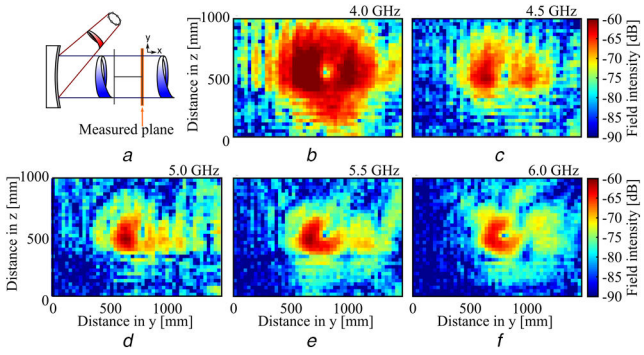

Fig. 6 *Measured field intensity from the 4–6 GHz field scan, $l = -1$ OAM mode beam in the y–z plane*

(a) Schematic diagram showing the measured plane. The scan was taken at 3.0 m away from microwave mirror (Plane 2), ***(b)*** Field intensities for 4 GHz, ***(c)*** Field intensities for 4.5 GHz, ***(d)*** Field intensities for 5 GHz, ***(e)*** Field intensities for 5.5 GHz, ***(f)*** Field intensities for 6 GHz

shows that of a singular helical pattern – characteristic of an OAM $l = \pm 1$ beam. As the beam size is reduced (as shown in Fig. 4), the diameter of the helical phase pattern is reduced, but the characteristic structure is still present. This phase pattern confirms that the collimation method had not altered the structure of the beam, aside from reversing the handedness, and therefore could be used as a feasible method of propagating an OAM into free space.

Fig. 6 shows the measured field intensity for the *y–z* plane at the position Plane 2. The scan at Plane 2 was taken 3.0 m away from the microwave mirror, Fig. 6*a* shows a schematic of the scan location. As expected from the analysis of Fig. 3, the field intensity shown for Plane 1 (Fig. 4) and Plane 2 (Fig. 6) closely match, with minimal spread in the *y–z* plane.

For completeness, Fig. 7 shows the phase patterns for the range of frequencies at Plane 2. Once more the rotation of a single helix is observed for an OAM $l = -1$ beam. In this case, Figs. 5 and 7 only differ due to the rotation of the beam with propagation, further showing that the OAM characteristics have been unaltered by the collimation process. The results presented in Figs. 3–7 have shown that a radio-frequency OAM beam can be collimated – in this case using a spherical microwave mirror – without removing the essential OAM characteristics.

A quantitative comparison between the standard generated beam and the collimated beam at 5 GHz is shown in Fig. 8. The beam diameter is shown as a function of distance in the *x* direction. The lines of best fit were determined using a first-order polynomial fit, thus showing a beam divergence of 36.6° for the standard beam (Fig. 8*a*) and 1.2° for the collimated beam (Fig. 8*b*). The first point of standard beam is measured after the beam has propagated for 0.5 m, compared to the first point for the collimated beam has propagated for 1.6 m from the mirror (in addition to 1.8 m to the mirror from the UCA). The difference in initial propagation

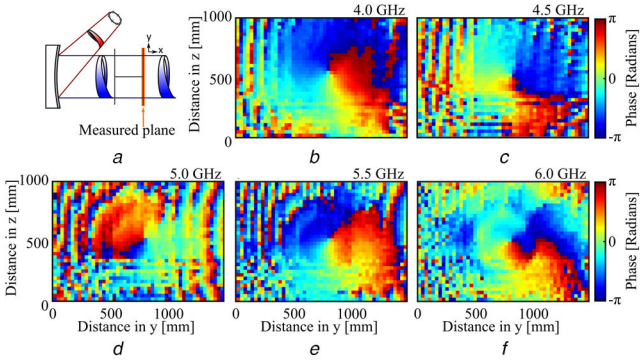

Fig. 7 *Measured phase pattern from the 4–6 GHz field scan, $l = -1$ OAM mode beam in the y–z plane*

(a) Schematic diagram showing the measured plane. The scan was taken at 3.0 m away from microwave mirror (Plane 2), ***(b)*** Field intensities for 4 GHz, ***(c)*** Field intensities for 4.5 GHz, ***(d)*** Field intensities for 5 GHz, ***(e)*** Field intensities for 5.5 GHz, ***(f)*** Field intensities for 6 GHz

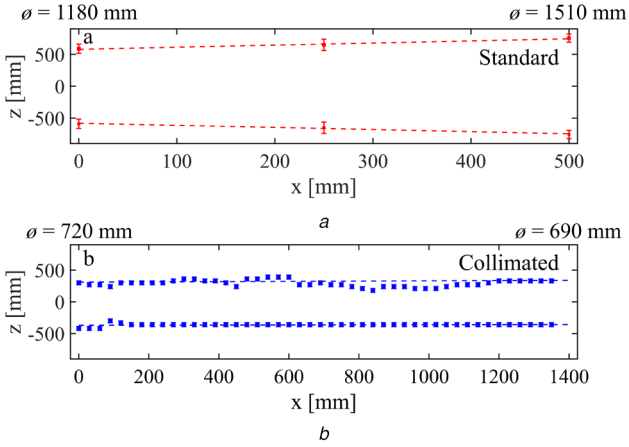

Fig. 8 *Beam diameter as a function of distance (in the x direction) for*

(a) Standard $l = +1$ OAM mode beam at 5 GHz, ***(b)*** Collimated $l = -1$ OAM mode beam at 5 GHz centred on the average null position. The lines of best fit was determined using a first-order polynomial fit

distance further demonstrates the effectiveness of the beam collimation technique.

Since the phase of an OAM beam exhibits a distinct behaviour, it is possible to determine the purity of the OAM mode by analysing the phase change around the beam's circumference. An approximation to the phase gradient commonly used is the measurements of the phase difference between two points on a circle [15, 23, 24].

A schematic of this method is shown in Fig. 9 (inset), where R is the radius of the circle; ϕ_1 and ϕ_2 are the measured beam phases; and the angle between the two measurements is given by $\beta_{1,2}$. The estimated received OAM mode can be calculated using the expression

$$l_{\mathrm{R}} = \frac{\phi_1 - \phi_2}{\beta_{1,2}}. \tag{1}$$

Using $R = 100 \pm 10$ mm, the estimates of the received modes were calculated and are shown in Fig. 9. To distinguish between OAM modes, the received mode should fall within ±0.5 of an integer mode number.

Fig. 9*a* shows the estimated received OAM mode of the standard generated beam. As predicted, the received mode $l = +1 \pm 0.5$ over the full probed region. Fig. 9*b* shows the received mode number for the frequency range (4.0–6.0 GHz) for Plane 2. As previously stated, it is expected that the OAM mode will change sign with the collimation technique. Typically, for all frequencies over the probed region the estimated mode is $l = -1 \pm 0.5$.

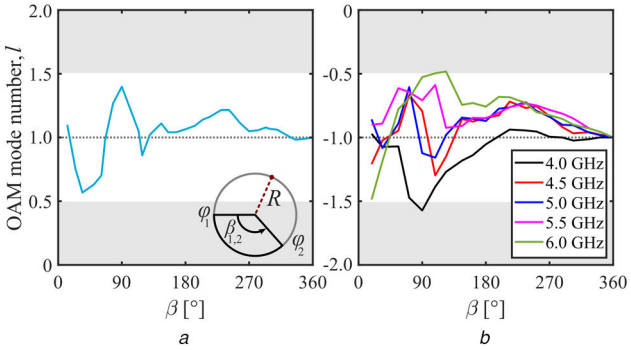

Fig. 9 *Estimated OAM mode purity calculated using the approximate phase gradient method. The fixed radius used was* $R = 100 \pm 10\,mm$
(a) Estimated OAM mode for the standard (non-collimated) OAM beam, ***(b)*** Estimated OAM mode for frequencies between 4.0 and 6.0 GHz at Plane 2, for the collimated beam. The inset shows a schematic diagram of the probing method

For small angular separations, this method results in a poor estimation of the mode, due to this method being an approximation to the full phase gradient method [25]. Nevertheless, this investigation further shows that the collimation method has not affected the OAM characteristics of the propagating beam.

4 Conclusion

The presented work focused on profiling the radio beam transmitted from an 8-element uniform circular. The array consisted of eight 5 GHz WiFi antennas uniformly spaced in a circular array. The work focused on the field intensity and phase for the $l = -1$ OAM mode for a broad range of frequencies (4–6 GHz). The transmitted beam was then collimated using a spherical microwave mirror and directed towards a field scanner, where the beam was probed with a receiver antenna. The field intensity and phase were scanned in three locations: the x–y plane, and two y–z planes separated so as to be 1.4 m apart. The scans showed that, for the chosen frequency range, the divergence due to the vortex centre was minimal as the beam propagated. The phase pattern was also shown in the scans to be unaffected by the collimation method. An investigation into the OAM mode purity also shows minimal distortion of the carried OAM mode. For a comparison, scans of a standard $l = +1$ OAM mode beam (generated from the same UCA) were presented to visualise and compare the divergence of the beam. It was shown that using this setup enabled the divergence to be reduced from 36.6° to 1.2°. An investigation into the OAM mode purity was also conducted to ensure that this method had a minimal effect on the OAM characteristics of the beam.

This investigation has shown that an OAM beam can be collimated by using a simple spherical microwave mirror whilst retaining the characteristics associated with an OAM beam. This paves the way for realising OAM radio for applications that require larger ranges, such as wireless communications, and potential radio astronomy experiments.

5 Acknowledgments

This research was partially funded by HM Govt, Dept for Transport (T-TRIG), The Open University School of Engineering and Innovation. TDD was at The Open University when measurements were conducted. Internal funding was provided by the Innovation & Improvement internal investment scheme within QinetiQ Ltd. This work was also supported by the UK Engineering and Physical Sciences Research Council Prosperity Partnership, TEAM-A (EP/R004781/1).

6 References

[1] Poynting, J.H.: 'The wave motion of a revolving shaft, and a suggestion as to the angular momentum in a beam of circularly polarised light', *Proc. R. Soc. Lond. A*, 1909, **82**, (2), pp. 560–567
[2] Allen, L., Beijersbergen, M.W., Spreeuw, R.J.C., *et al.*: 'Orbital angular momentum of light and the transformation of Laguerre-Gaussian laser modes', *Phys. Rev. A*, 1992, **45**, (11), pp. 8185–8189
[3] Beijersbergen, M.W., Coerwinkel, R.P.C., Kristensen, M., *et al.*: 'Helical-wavefront laser beams produced with a spiral phaseplate', *Opt. Commun.*, 1994, **112**, (5–6), pp. 321–327
[4] Simpson, N.B., Dholakia, K., Allen, L., *et al.*: 'Mechanical equivalence of spin and orbital angular momentum of light: an optical spanner', *Opt. Lett.*, 1997, **22**, (1), pp. 52–54
[5] Molina-Terriza, G., Torres, J.P., Torner, L.: 'Twisted photons', *Nat. Phys.*, 2007, **3**, pp. 305–310
[6] Thidé, B., Then, H., Sjöholm, J., *et al.*: 'Utilization of photon orbital angular momentum in the low-frequency radio domain', *Phys. Rev. Lett.*, 2007, **99**, (8), pp. 1–4
[7] Genevet, P., Lin, J., Kats, M.A., *et al.*: 'Holographic detection of the orbital angular momentum of light with plasmonic photodiodes', *Nat. Commun.*, 2012, **3**, pp. 1275–1278
[8] Mahmouli, F.E., Walker, S.D.: '4-Gbps uncompressed video transmission over a 60-GHz orbital angular momentum wireless channel', *IEEE Wirel. Commun. Lett.*, 2013, **2**, (2), pp. 223–226
[9] Thidé, B., Tamburini, F., Mari, E., *et al.*: 'Radio beam vorticity and orbital angular momentum', arXiv Preprints, arXiv:1101.6015 [astro-ph.IM], 2011, pp. 4–6
[10] Yan, Y., Xie, G., Lavery, M.P.J., *et al.*: 'High-capacity millimetre-wave communications with orbital angular momentum multiplexing', *Nat. Commun.*, 2014, **5**, pp. 1–9
[11] Vourch, C.J., Allen, B., Drysdale, T.D.: 'Planar millimetre-wave antenna simultaneously producing four orbital angular momentum modes and associated multi-element receiver array', *IET Microw. Antennas Propag.*, 2016, **10**, (14), pp. 1492–1499
[12] Maccalli, S., Pisano, G., Colafrancesco, S., *et al.*: 'Q-plate for millimeter-wave orbital angular momentum manipulation', *Appl. Opt.*, 2013, **52**, (4), pp. 635–639
[13] Mohammadi, S.M., Daldorff, L.K.S., Bergman, J.E.S., *et al.*: 'Orbital angular momentum in radio – a system study', *IEEE Trans. Antennas Propag.*, 2010, **58**, (2), pp. 565–572
[14] Edfors, O., Johansson, A.J.: 'Is orbital angular momentum (OAM) based radio communication an unexploited area?', *IEEE Trans. Antennas Propag.*, 2012, **60**, (2), pp. 1126–1131
[15] Drysdale, T.D., Allen, B., Stevens, C., *et al.*: 'How orbital angular momentum modes are boosting the performance of radio links', *IET Microw. Antennas Propag.*, 2018, **12**, (10), pp. 1625–1632
[16] Padgett, M.J., Miatto, F.M., Lavery, M.P.J., *et al.*: 'Divergence of an orbital-angular-momentum-carrying beam upon propagation', *New J. Phys.*, 2015, **17**, pp. 1–5
[17] Tamburini, F., Thidé, B., Mari, E., *et al.*: 'Encoding many channels on the same frequency through radio vorticity: first experimental test', *New J. Phys.*, 2012, **14**, pp. 1–17
[18] Allen, B., Drysdale, T.D., Zhang, S., *et al.*: 'Reduction of orbital angular momentum radio beam divergence using a 3D printed planar graded index lenses'. 12th European Conf. on Antennas and Propagation, London, UK, April 2018, pp. 83–86
[19] Allen, B., Simmons, D., Drysdale, T.D., *et al.*: 'Performance analysis of an orbital angular momentum multiplexed amplify-and-forward radio relay chain with inter-modal crosstalk', *R. Soc. Open Sci.*, 2019, **6**, (1), pp. 1–9
[20] Maity, S., Singha, K., Debnath, P., *et al.*: 'Textiles in electromagnetic radiation protection', *J. Saf. Eng.*, 2013, **2**, (2), pp. 11–19
[21] Stutzman, W.L., Thiele, G.A.: '*Antenna theory and design*' (John Wiley & Sons, Hoboken, NJ, USA 2012)
[22] Berry, S.J.: 'Microwave surface waves on metasurfaces with planar discontinuities'. PhD thesis, University of Exeter, 2014
[23] Mohammadi, S.M., Daldorff, L.K.S., Forozesh, K., *et al.*: 'Orbital angular momentum in radio: measurement methods', *Radio Sci.*, 2010, **45**, (4), pp. 1–14
[24] Chen, J., Liang, X., He, C., *et al.*: 'High-sensitivity OAM phase gradient detection based on time-modulated harmonic characteristic analysis', *Electron. Lett.*, 2017, **53**, (12), pp. 812–814
[25] Berkhout, G.C.G., Beijersbergen, M.W.: 'Method for probing the orbital angular momentum of optical vortices in electromagnetic waves from astronomical objects', *Phys. Rev. Lett.*, 2008, **101**, (10), pp. 1–4